Hyaluronic acid hydrogel with growth factor sequestering capability for promoting in vivo bone regeneration

Authors: Hong Ji Yan[1], Tommaso Casalini[2], Gry Hulsart-Billström[3], Shujiang Wang[4], Oommen P. Oommen[5], Matteo Salvalaglio[6], Sune Larsson[3], Jöns Hilborn[4], and Oommen P. Varghese [4,*]

Affiliations:

[1]Royal Institute of Technology, Stockholm, SE-106 91, Stockholm, Sweden.

[2]Institute for Chemical and Bioengineering, Department of Chemistry and Applied Biosciences, ETH Zurich, Vladimir-Prelog-Weg 1, 8093 Zurich, Switzerland.

[3]Department of Orthopedics, Uppsala University, Uppsala, Sweden.

[4] Institute of Polymer Chemistry, Department of Chemistry, Uppsala University, SE-751 21 Uppsala, Sweden.

[5]Bioengineering and Nanomedicine Lab, Faculty of Biomedical Sciences and Engineering & Biomeditech Institute, Tampere University of Technology, Tampere, Finland, 33720

[6]Department of Chemical Engineering, University College London, London WC1E 7JE, UK

- E-mail: Prof. Oommen P. Varghese oommen.varghese@kemi.uu.se

One Sentence Summary: Tuning hyaluronic acid backbone protonation state in a 3D-hydrogel regulates BMP-2 release and osteogenic induction in vivo.

Abstract

Synthetic scaffolds that possess an intrinsic capability to store, protect and sequester sensitive growth factors is a primary requisite for developing successful tissue engineering strategies. Growth factors such as recombinant human bone morphogenetic protein-2 (rhBMP-2) are highly susceptible to premature degradation and to provide meaningful clinical outcome require high doses. Such high doses manifest undesired side effects. We have discovered a unique and straightforward strategy that stabilize and sequester rhBMP-2 by enhancing the molecular interactions with an extracellular matrix component, namely hyaluronic acid (HA). We found that by tuning the protonation and deprotonation states of carboxylic acid residues of HA in a covalently crosslinked hydrogel, resulted in a controlled release of active BMP-2. At neutral pH, BMP-2 release is primarily governed by Fickian diffusion through the hydrogel, whereas at acidic pH both diffusion and electrostatic interactions between hyaluronic acid and BMP-2 become important. The molecular interaction of BMP-2 with HA at different pH was also demonstrated using molecular dynamic simulations, which corroborates with the in vitro protein release profile. Our results were equivocally validated in an in vivo rat ectopic model with rhBMP-2 loaded hydrogels, which demonstrated superior bone formation with acidic hydrogel compared to the neutral counterpart. We believe this study provides new insight on growth factor

stabilisation within scaffolds and highlights the therapeutic potential of engineered ECM mimetic matrices for the delivery of rhBMP-2 and may help to curtail the adverse side effects associated with the high dose of the growth factor currently in clinical practice.

Introduction

Strategies involving delivery of growth factors using scaffolds are widely explored for regenerative medicine applications (*1*). They are particularly important for treating large bone defects (critical size) that fail to heal by themselves. Large bone defects are commonly treated using autologous bone grafting where healthy bone tissue from patient is harvested and implanted at the defect site. However, lack of transplantable bone, donor site morbidity and lack of good quality bone tissue in elderly patients (*2*) results in suboptimal clinical outcome . Thus, regenerative medicine-based approaches are developed in order to accelerate bone healing. To differentiate bone-forming mesenchymal stem (progenitor) cells towards osteoblasts, specific growth factors are needed, where the most potent are the morphogenetic proteins (BMPs) namely BMP-2 and BMP-7 (*3*). Recombinant human (rh) version of both these proteins are approved for clinical use by FDA (US Food and Drug Administration) as well as EMA (European Medicines Agency), however, due to severe risks of side-effects, rhBMP-7 also called OP-1 (Osteogenic Protein-1) is withdrawn from the market whereas rhBMP-2 (InductOs®) is currently having limited sale in Europe. Recently, an extensive debate has taken place on the clinical use of rhBMP-2 since several complications are observed in patients, which include acute respiratory, neurological and inflammatory complications (*4*). This led the FDA to issue a public health notification of life-threatening complications (*5*). The primary cause of such severe complications is due to the supraphysiological dose of rhBMP-2 (1.5 mg mL^{-1}) that is used clinically with a collagen sponge-based carrier. Such high doses are needed because collagen-based scaffolds are not effective in stabilizing rhBMP-2 in vivo (*6*). It is interesting to note that at high doses, BMP-2 induces adipogenic differentiation of MSCs by activating *PPAR*-γ (peroxisome proliferator-activated receptors) pathway (*7*) and at the same time activates bone resorbing osteoclasts (*8*), resulting in poor quality bone.

BMP-2 is an unstable protein that easily undergoes denaturation resulting in loss of function. We have recently confirmed that rhBMP-2 undergoes aggregation at physiological pH and adheres to hydrophobic surfaces such as cell culture plastics and Eppendorf tubes (*9*). Recently, this association of BMP-2 to hydrophobic surfaces has been utilized to develop nanocarriers for efficient delivery of the protein in vivo (*10*). In living systems, soluble forms of growth factors are stabilized by the biopolymers present in the ECM (extracellular matrix) that regulate dynamic stem cell niche (*11*). Thus several researchers, including our group, have attempted to develop ECM mimetic scaffolds to deliver functional BMP-2 in vivo (*12, 13*). Several strategies have been employed to increase the bioavailability and stability of this protein. These strategies include engineering recombinant protein with a specific ECM binding motif to control sequestration (*14*), immobilizing protein by covalent conjugation (*15*), electrostatic binding to modified surfaces (*16*), and incorporating specific BMP-2 binding peptides or glycosaminoglycans (GAGs) such as heparan sulfate into the scaffold (*17*). Although these strategies are promising, they are cumbersome entailing complex bioengineering steps that often result in the loss of function due to covalent/electrostatic immobilization. It is noteworthy that rhBMP-2 is stable and remains biologically active when constituted at acidic pH (~4.5) resulting in efficient ectopic bone formation (*18*). Scaffolds also play a crucial role in dictating the bioactivity of this growth factor. The BMP-2 complexed to different scaffolds may result in

either stimulatory or inhibitory effects in bone formation. The stimulatory effect is attributed to the increase in BMP-2 half-life by minimizing interaction with BMP antagonist noggin (*17*), whereas the inhibitory effect is due to inefficient binding of BMP-2 to its cognate receptor (*19*). BMP-2 complexing biomolecules such as HA, chondroitin sulfate and heparin also have a unique biological function related to the coagulation and complement system of the blood that also affect the biological outcome (*20*). These results prompted us to design a BMP-2 sequestering 3D scaffold without using any special complexing agents that could enhance the stability and bioavailability of BMP-2.

In this article, we describe a novel strategy to engineer HA hydrogel having different carboxylic acid protonation states such that it differentially interact with rhBMP-2 and regulate controlled release kinetics of bioactive BMP-2. In order to gain insight on the influence of backbone protonation of HA to bind BMP-2 within the HA-gel, we performed a multiscale modeling approach combining fundamental mass balances with simulations at the molecular level. The results of the computational analysis as well as the in vitro release experiments were further corroborated by in vivo experiments in a rat ectopic model. In summary, we present a new insight in material design that is simple and translatable, which could pave the way to develop safe and cost-effective regenerative medicine strategies.

Results

Hydrogel preparation and characterization

We fabricated two HA hydrogels having different pH, by modifying the synthetic procedure from our previously optimized hydrazone crosslinked hydrogel that was obtained by mixing carbohydrazide modified HA derivative with aldehyde modified HA derivative (*13*). The hydrazone crosslink exhibited excellent stability at physiological pH, which is attributed to the extensive delocalization of charges over the urea-type linkage. To prepare hydrogel components having acidic pH, we synthesized the HA derivatives as previously reported and performed dialysis under acidic pH (~3). However, to develop neutral gels, we neutralized the purified hydrogel components to pH 7.4 by using 0.1 M NaOH and subsequently dialysed them against water (see experimental section for details). Both HA hydrogels were prepared by mixing 1:1 ratio (*v:v*) of the HA-aldehyde and HA-hydrazide components in phosphate buffer saline (PBS, pH 7.4). The final pH of the hydrogel was determined by measuring the pH of the gel components before mixing and was found to be ~4.5 for acidic hydrogel and ~7 for neutral gel. These HA hydrogels were subjected to rheological assessment before and after swelling in phosphate buffer. Time-sweep rheological evaluation was performed to determine the gel point of the two-hydrogel systems, *i.e.*, pH 4.5 (acidic) and pH 7 (neutral) HA-hydrogels. These experiments indicated that the acidic hydrogel had a shorter gelation time (90 seconds) whereas the neutral hydrogel took 13 minutes to reach the gel point (**Figure 1A, B**). Gel characteristics after complete crosslinking (i.e., after 24 h of curing) reveals that the neutral hydrogel was more rigid (~300 Pa after swelling) than the acidic hydrogel (**Figure 1C, D and Table 1**). This was also reflected in the calculated average molecular weight between crosslinks (Mc) and the pore size (ξ), which shows that neutral hydrogel had lower Mc and smaller ξ (*13*). However, the acidic and neutral gels had similar swelling and hyaluronidase (HAse) mediated enzymatic degradation rate (**Table 1**).

In vitro release of bioactive rhBMP-2 from acidic and neutral HA hydrogels

Next, we evaluated the release of functional BMP-2 from our HA-gels. Even though it is generally accepted that association of BMP-2 with the scaffold and its controlled release is important, there exist some disagreements on the physiological dose that is needed to be released at different stages of bone formation. Some researchers suggest that initial burst release followed by sustained release is important (*21*) whereas other reports indicate that controlled release is the key for effective bone induction (*6*). Nevertheless, it is generally accepted that high burst release as observed from collagen sponge is not desirable (*6, 22*). To evaluate the differential binding and release properties of functional rhBMP-2 from the two hydrogel systems having different pH, we performed in vitro ALP assay in BMP-responsive mouse stromal cell line (W-20-17) from the released media obtained as a function of time. This indirect approach is superior to conventional approach as it estimates only the biologically functional BMP-2 released from the gels. These experiments revealed that the acidic hydrogels showed a linear increase of ALP activity from day 1 to day 28. However, rhBMP-2 released from the neutral hydrogels exhibited initial burst release with nearly 65% of active rhBMP-2 released by day 7 (**Figure 2**).

To understand the differences in release rate of rhBMP-2 from the two types of HA hydrogels, we performed modeling experiments by employing the fundamental mass balances, *i.e.* Fick's second law of diffusion written in cylindrical coordinates and considering axial coordinate only (**Equation 1**):

$$\frac{\partial C_{protein}}{\partial t} = D\frac{\partial^2 C_{protein}}{\partial z^2} \tag{1}$$

$C_{protein}$ is protein concentration in the HA hydrogel, D is the diffusion coefficient and z is HA vertical hydrogel axis.

Since the experiment was performed in a trans-well setup, the protein could be released only through the bottom surface of the HA hydrogel; therefore, only the axial coordinate was considered in the equation. The diffusion coefficient was fitted in order to best reproduce the experimental data, assuming that after 28 days a complete release has been achieved. This resulted in D values of 2.19×10^{-7} cm^2 s^{-1} and 4.11×10^{-7} cm^2 s^{-1} for acidic and neutral hydrogels, respectively. Comparison between simulated and experimental results is shown in **Figure 2**. These results suggest that the protein release at physiological pH can be reasonably described as a Fickian behavior (where the molecular diffusion is the most important phenomenon). On the other hand, BMP-2 release at pH 4.5 exhibits a substantial deviation from Fickian behavior, indicating that molecular diffusion is not the only mechanism affecting release rate (**Figure 2**).

We, therefore, proposed a new model to understand the protein release characteristics at acidic pH, assuming that the attainment of interactions between the protein and the matrix can influence BMP-2 diffusion within the hydrogel. In this framework, the protein can be bound to the polymer matrix or move freely in the water-filled pores, resulting in a release profile that involves both molecular diffusion and protein desorption from hydrogel chains. It is also assumed that before release onset, bound and free protein fractions are at equilibrium. A mass balance for unbound (**Equation 2**) and bound protein (**Equation 3**) is described as follows:

$$\frac{\partial C_{protein,u}}{\partial t} = D\frac{\partial^2 C_{protein,u}}{\partial z^2} + k_{des}\left(C_{protein,eq} - C_{protein,u}\right) \tag{2}$$

$$\frac{\partial C_{protein,b}}{\partial t} = -k_{des}\left(C_{protein,eq} - C_{protein,u}\right) \tag{3}$$

k_{des} is desorption constant, $C_{protein,b}$ is adsorbed protein concentration, $C_{protein,u}$ is protein concentration in water filled pores, and $C_{protein,eq}$ is the protein concentration in the water-filled pores at equilibrium with the bound protein.

Diffusion coefficient D, desorption constant k_{des} and protein concentration at equilibrium $C_{protein,eq}$ have been fitted against experimental data at pH 4.5 which resulted in D, k_{des} and $C_{protein,eq}$ values to be 1.2×10^{-6} cm^2 s^{-1}, 3.47×10^{-6} s^{-1} and 7.14×10^{-4} µmol cm^{-3} respectively. Comparison between experimental and calculated data is shown in **Figure 2**, which indicates that our proposed model is in a good agreement with the experimental protein release profile at acidic pH. The obtained interaction parameters with our protein release experiments are summarized in **Table 2**.

Fitted parameters allowed qualitative estimation of the characteristic time scale for both desorption (τ_{des}) and diffusion (τ_{diff}) phenomena:

$$\tau_{des} = \frac{1}{k_{des}} \tag{4}$$

$$\tau_{diff} = \frac{z_{axis}^2}{D} \tag{5}$$

The obtained values for τ_{des} and τ_{diff} are 2.88×10^5 s and 2.99×10^5 s respectively. The reliability of the calculated diffusion coefficients was determined by estimating the corresponding value in water solution. Since the experimental diffusivity of BMP-2 in aqueous environment is not reported so far, we employed the equation proposed by Hem *et al.* (*23*):

$$D = \frac{6.85 \cdot 10^{-15} T}{\eta \sqrt{M^{\frac{1}{3}} R_G}} \tag{6}$$

Where T is the absolute temperature, η is water viscosity (equal to 0.682 cP, at 37 °C), M is protein molecular weight (equal to 28,000 g mol^{-1}) and R_G is the radius of gyration (set equal to 2.05 nm, computed from molecular dynamics simulations, *vide infra*). This allowed obtaining a diffusion coefficient value equal to 1.25×10^{-6} cm^2 s^{-1}.

The development of interactions between the protein and the matrix was investigated using simulations at a molecular scale, according to the adopted multiscale modeling approach. To estimate the affinity between HA and rhBMP-2 at neutral and acidic pH condition, we performed molecular dynamics simulations. For this purpose, BMP-2 atomic coordinates were taken from crystallographic structure available in the literature (PDB code: 1REW (*24*)) and the protonation states as a function of pH were evaluated by means of H++ software (*25*). The system under investigation was modeled with the BMP-2 protein interacting with a model chain of HA composed of 6 monomers (*i.e.* 12 disaccharide units). Glucuronic acid moieties are assumed to be fully dissociated at both considered pH values, as the pK_a value for HA is approximately 3 (*26*).

The structures of BMP-2–HA complexes input guess geometries for simulations were obtained by means of molecular docking. As described in the literature, BMP-2 exhibits a *'wrist-knuckle'* 3D structure where the 'wrist' epitope of BMP-2 binds to the type I receptors (*24, 27*), while the 'knuckle' epitope binds to the type II receptors presented on the cell surface (*28*). Wrist and knuckle epitopes were considered as potential binding sites in the docking procedure, as well as the upper and lower portion of the protein. To simplify the nomenclature, the input

arrangement obtained through docking, are arbitrarily named as wrist (**Figure 3A**), knuckle (**Figure 3B**), upper (**Figure 3C**) and lower (**Figure 3D**) geometries depending on the structure.

For each input guess structure, 75 ns molecular dynamics simulation was performed at 310 K and 1 atmosphere with explicit water molecules and ions to reproduce the physiological environment (PBS). The interaction energy between BMP-2 and HA model chain was computed using the last 25 ns utilizing Molecular Mechanics Poisson Boltzmann Surface Area (MMPBSA) approach. Results are summarized in **Table 3**, which includes interaction energy values ΔE along with electrostatic and Van der Waals contributions.

The computed energies demonstrated that the electrostatic interactions between the solute and the matrix are more favorable at pH 4.5 than at pH 7 (except the lower complex). To explain the obtained results, we computed the electrostatic potential on protein surface using representative snapshots from simulations (**Figure 4A** and **4B**). Blue colored areas represents positively charged regions, while the red ones indicate negatively charged regions; the electrostatic potential is expressed in the dimensionless unit k_BeT^{-1}, where k_B is Boltzmann constant, e is electron charge, and T is the absolute temperature. The overall protein charge is equal to +4 and -8 at pH 4.5 and 7 respectively. On one hand, this implies the presence of large positively charged areas at pH 4.5 (**Figure 4A**) that could favor the binding of negatively charged HA (**Figure 4C**). On the other hand, the negative charge of BMP-2 at pH 7 can hinder the formation of stable complexes. Representative complex structures at pH 4.5 and pH 7 are shown in **Figure 5** and **Figure 6** respectively, along with electrostatic potential on protein surface.

This analysis was complemented by computing hydrophobic patches located on protein surface by means of Spatial Aggregation Propensity (SAP) algorithm proposed by Chennamsetty *et al.* (*29*). As shown in **Figure 7**, red-colored areas represent the hydrophobic regions, whereas the blue regions indicate the hydrophilic domains. The neutralization process was qualitatively simulated by starting from the equilibrated complexes obtained at pH 4.5 followed by changing the protonation state of the protein to pH 7. Additional 75 ns molecular dynamics simulations were performed to obtain equilibrated structures and the last 25 ns of each trajectory were used for computing interaction energy using the MMPBSA approach, as summarized in **Table 4**.

These experiments reveal that the obtained interaction energies are less favorable at neutral pH than the ones at pH 4.5, due to non-favorable electrostatic interactions. The lower complex is an exception since it involves a positively charged binding area even at pH 7. Interestingly, our simulation experiments also demonstrate that the change in protonation state upon neutralization results in a rearrangement of complex structures to minimize the unfavorable electrostatic interactions and enhance Van der Waals interactions. Such a complex stabilization effect due to Van der Waals interactions are not observed in neutral hydrogels.

In vivo osteogenesis of HA hydrogels containing rhBMP-2

To evaluate the osteogenic potential of the two rhBMP-2-loaded hydrogels, we performed in vivo subcutaneous implantation of the HA hydrogels with low doses of rhBMP-2 (4 μg rhBMP-2 in 200 μl HA hydrogels which correspond to 20 μg/mL) in a rat model. In vivo bone induction in terms of bone volume was quantified in live animals using dynamic μCT employing temporal scans to follow the same animals. Interestingly, the acidic HA hydrogels displayed detectable bone formation already after two weeks, whereas the neutral HA hydrogels showed detectable bone formation only by week six (**Figure 8A**). In addition, the acidic HA hydrogels produced

significantly much larger bone volume as compared to the neutral hydrogels with the same BMP-2 concentrations. This was evident at all time points tested and after eight weeks bone volume were 62.69 ± 22.09 (mm^3) and 12.44 ± 3.16 (mm^3) in the acidic hydrogels and 12.44 ± 3.16 (mm^3) in the neutral hydrogels (**Figure 8A**).

The rats were sacrificed at week 8 and the ectopic bone was harvested. Samples were scanned individually by μCT ex vivo. Both the representatives of 3D construction images of the samples (**Figure 8B and 8C**) and the statistical analysis revealed that bone volume was significantly larger for acidic hydrogel implants (65 mm^3) as compared to that of the neutral hydrogel implants (18 mm^3) (**Figure 8D**). These values corroborate with the bone volume determined using dynamic in vivo μCT mentioned above. The histological evaluation was carried out on the ectopic bone explants of the acidic and neutral hydrogels. Representatives of cross sections stained by H&E and Masson's trichrome revealed that newly formed bone induced by acidic hydrogel with rhBMP-2 (**Figure 9A, B, C, D**) exhibited a matured bone tissue with abundant adipocytes 'a' as in a bone marrow and mineralized bone 'b' with abundant osteoblasts (**Figure 9**. The neutral hydrogel carrying rhBMP-2 however, induced neo bone (**Figure 9E, F, G, H**) with less mineralized tissue. We also observed some remnant of hydrogels in these gels, indicated as 'g' (**Figure 9**). It is noteworthy that we did not observe any inflammatory cells (**Figure 9**) or fibrotic tissue in the neo bone induced by both hydrogels with rhBMP-2.

Discussion

Controlled delivery of growth factors as drugs for regenerative medicine applications primarily relies on the carrier that is used. These carriers have to be biocompatible and should increase the pharmacokinetic and pharmacodynamics characteristics of the drug molecule. One such growth factor is BMP-2 that has been clinically used for bone regeneration applications. There are several challenges to overcome to use BMP-2 as a safe therapeutic agent, such as, minimize required dosage, control drug release profile from the scaffold, improve the interaction of BMP-2 with its cognate cell-surface receptors as well as increase its half-life. In this article, we present a novel strategy to stabilize rhBMP-2 and control its release to allow improved bone regeneration at lower doses.

As a carrier of rhBMP-2 that differentially stabilizes protein, we envisioned to exploit the chemical behavior of the carboxylic acid functionality that is naturally present in HA, a natural component of ECM. Since the pK_a of HA-carboxylate is around 3, designing injectable HA-based hydrogel having ionizable carboxylic acid or its conjugate base (carboxylate) should render different stabilization of rhBMP-2. We have previously shown that rhBMP-2 remain stable at pH ~4.5 (also recommended in the product description) but undergo slow aggregation at physiological pH (*9*). Thus, hydrogels having differential protonation states (or inherent pH) should demonstrate differences in BMP-2 stability and bioactivity. To test this hypothesis, we selected our previously optimized HA-based hydrazone-crosslinking chemistry (*13*) but changed the material preparation protocol to develop the acidic and neutral hydrogel. Of note, this "click-type" crosslinking chemistry is superior to the conventional hydrazone chemistry as it provides for significantly improved hydrolytic stability of the formed hydrazone linkages. The hydrogel thus obtained demonstrated similar physical properties as well as susceptibility to hyaluronidase-mediated degradation. The rheological characterization of the acidic and neutral HA hydrogels showed similar gel characteristics as judged by modulus, mesh size and swelling ratio (**Table 1**),

however, the gel point was reached at a shorter time point with the acidic gel as compared to that of the neutralized gel (**Figure 1A, B**). This is anticipated, as hydrazone formation is acid catalyzed, and at neutral pH such a reaction can be catalyzed by carboxylic acids residues present in HA backbone, as reported recently by our group (*30*).

We further evaluated the in vitro release of biologically active rhBMP-2 from the two-hydrogel systems using ALP assay in W20-17 cells. Interestingly, the 28 days release experiments showed two different release profiles of the bioactive rhBMP-2. To better understand the rhBMP-2 release characteristics, we subsequently modeled protein release by means of fundamental mass balances, *i.e.* by employing Fick's second law of diffusion. Specifically, we estimated the diffusion coefficient of rhBMP-2 by fitting the experimental protein release data. As shown in **Figure 2**, this approach led to satisfactorily results for the release at neutral pH, while the agreement was quite poor at the acidic pH, confirming a substantial deviation from Fickian behavior. This can be attributed to the molecular interactions between the protein and the HA-chains within the hydrogel i.e., adsorption parameters that is not accounted for in the diffusion model. We therefore employed a diffusion/desorption model to describe the protein release, which is now due to the sum of two effects: diffusion of the free solute and irreversible desorption of the bound protein from HA chains. The desorption process is modeled as a first-order because of the low solute concentration. In this framework, the diffusion coefficient, the protein concentration (in the liquid-filled pores at equilibrium with the adsorbed one), and the desorption-constant are employed as fitting parameters. Such a fitting showed good agreement with the experimental release profile of rhBMP-2 at acidic pH. Assuming a uniform solute distribution, the initial protein concentration within the hydrogel is equal to 3.6×10^{-3} μmol cm^{-3}. According to model best fitting, at pH 4.5 the protein concentration in the hydrogel bulk phase at equilibrium with the bound one is equal to 7.14×10^{-4} μmol cm^{-3}. This indicates that before release onset, about the 80% of the protein is bound to the matrix, and solute concentration in the water-filled pores is substantially reduced and close to an infinite dilution condition.

The obtained diffusion coefficient is about one order of magnitude lower than the values computed considering only diffusion, at both pH 4.5 and pH 7. So far, there are no experimental data about BMP-2 diffusion coefficients in water or HA hydrogels. A representative reference value of BMP-2 diffusion in water at 37 °C at infinite dilution can be computed through available literature correlations, similar to the one proposed by Hem *et al.* (eq. 6) (*23*). Indeed, as mentioned, the low protein concentration inside the pores can be representative of an infinite dilution situation, which also implies a limited driving force for the diffusion out of the matrix. Moreover, the reduction of diffusion rate caused by HA is likely limited, since the mean mesh size is 12.4 nm for the acidic HA hydrogel, 11.6 nm for the neutral HA hydrogel being significantly larger than the 2.05 nm protein radius of gyration computed from the atomic coordinates taken from crystallographic structure.

Model parameters allowed computing characteristic time scales for diffusion and desorption, equal to 2.88×10^5 s and 2.99×10^5 s, respectively. Such values are very close to each other, thus suggesting that desorption and diffusion have the same importance on the overall release behavior at pH 4.5, while at pH 7 the diffusion process dominates.

To investigate the interactions between the protein and the matrix, we performed molecular dynamics simulations. For the sake of simplicity, the system is modeled as BMP-2 interacting with a model chain of HA composed of six repeat units (that is, 12 sugar rings) in

aqueous environment having physiological salt concentrations. Since experimental structures of complexes between BMP-2 protein and HA are not available in the literature, molecular docking procedure was necessary to obtain consistent guess geometries; this resulted in four different arrangements for each considered pH, which were used as input for molecular dynamics simulations. The affinity between the protein and the matrix was characterized by computing the interaction energies through MMPBSA approach. The obtained trend in energies demonstrates that the molecular interactions are more favorable at pH 4.5 due to the electrostatic contribution to the interaction energy (**Table 3**). Such interactions promotes binding at low pH while can hinder the formation of complexes in neutral conditions. This difference is related to the pH-dependent state of protonation. On the HA the carboxylate anions remains largely undissociated also at pH 4.5, as it has pK_a value of 3 (*26*).

Interestingly, at neutral pH the protein has a total charge of -8 (according to H++ calculations), which changes to +4 when the pH drops to 4.5 thus promoting interactions with the negatively charged HA. The protein was further characterized by calculating the electrostatic potential on the surface (**Figure 4A** and **4B**). These calculations showed that the net positive charge at low pH implies the presence of large regions with a positive electrostatic potential, which favors the binding through electrostatic interactions, as confirmed by MMPBSA calculations. As shown in **Figure 5**, in its binding pose HA preferably interacts with blue-colored regions, characterized by a positive electrostatic potential. On the other hand, because of the overall negative charge of the protein at pH 7, complex formation occurs through Van der Waals interactions involving hydrophobic patches on the protein, as shown in **Figure 7** as confirmed by the relevant Van der Waals contribution according to MMPBSA calculations. In such a system, the HA chain is arranged to minimize the electrostatic repulsion between negatively charged moieties (**Figure 6**).

We further investigated the molecular interactions between BMP-2 and the HA chain as a result of neutralization of acidic hydrogel. For this purpose, we selected the complex structures obtained at pH 4.5 and changed the protonation state of the protein to the corresponding one at pH 7. After additional 75 ns molecular dynamics simulations, interaction energies were computed by means of MMPBSA using the previous protocol. Notably, no unbinding events occurred, but complex geometries experienced a rearrangement aimed at minimizing electrostatic repulsion and enhancing Van der Waals interactions. The obtained interaction energies showed the same peculiarities at pH 7, namely a reduced affinity compared to pH 4.5 due to an unfavorable electrostatic contribution.

Despite such a marked alteration of its total charge, protein denaturation was not observed in the timespan of 50 ns for the isolated BMP-2 at pH 4.5. For the sake of completeness, it should be pointed out that in the employed protein input structure the coordinates of the first 11 amino acid residues are not available, since they are missing in the employed crystallographic structure. Each missing sequence contains four lysine and two arginine residues, which are expected to be protonated at both pH 4.5 and pH 7. This leads to a systematic underestimation of the overall protein charge, thus explaining the discrepancy between the BMP-2 charge at pH 7 and the experimental isoelectric point of BMP-2 (~8.2). Therefore, our results should be considered as lower level for binding affinities.

The insights we obtained through the multiscale modeling, the system behavior can be rationalized as follows. At neutral pH, the affinity between the matrix and the protein is due only to Van der Waals interactions, which must counter-balance the electrostatic repulsion since both

BMP-2 and HA exhibit an overall negative charge. Solute/matrix interactions are negligible; before release onset, all BMP-2 is available for release, which is due only to molecular diffusion. At acidic pH (*i.e.* 4.5), a high protein fraction is bound to the matrix because of electrostatic interactions. During the release, irreversible desorption from the HA occurs for two reasons. Firstly, BMP-2 in the water-filled pores diffuses out of the matrix and promotes desorption because of the deviation from adsorption equilibrium, and secondly neutralization weakens the mutual interactions and destabilizes the complexes. Therefore, at low pH BMP-2 release is due to the synergic effects of both molecular diffusion and desorption, which causes the deviation from the Fickian behavior.

To investigate if our improved molecular understanding has any implications in reality, we examined the potential of our injectable hydrogels to induce bone formation in an animal model. Implantation of the acidic and neutral hydrogels ectopically in a rat model, with a significantly low dose of rhBMP-2 (4 μg/200 μL of hydrogel), indeed confirmed our findings with surprising efficacy. The acidic hydrogels gave nearly twice the amount of bone tissue volume as compared to the neutral hydrogels after eight weeks, as determined by μCT analysis (**Figure 8**). This clearly shows that the controlled release of the rhBMP-2 plays a major role in in vivo bone induction. Since, we evaluated a cell-free hydrogel system, the acidic hydrogel (that eventually will get neutralized) should be capable of recruiting endogenous stem cells and promote osteogenic differentiation. We have recently investigated this aspect and found that there is indeed a unique cell recruitment pattern (stem cells, M1 and M2 macrophages) in the different hydrogel systems, with and without rhBMP-2 (*31*).

We further investigated the quality of neo bone by histochemical analysis. The H&E and Masson's trichrome staining indicated ectopic bone formation induced by both acidic and neutral hydrogels. Direct comparison of the two-hydrogel system clearly demonstrated better quality of ectopic bone with acidic gel as compared to that of the neutral gel. The bone tissue obtained from the acidic gel indicated well-mineralized bony structure with adipocytes as in bone marrow (**Figure 9A, B, C, D**), unlike the neutral counterpart (**Figure 9E, F, G, H**). We anticipated the acidic hydrogels influenced the release of bioactive rhBMP-2, which facilitated the bone formation.

Conclusions

We present here a novel strategy to fabricate HA gels such that it differentially interacts with the BMP-2 and regulate its release at physiological pH. The HA derivative having the carboxylic acid groups enhanced binding to BMP-2 whereas the conjugate base (carboxylate) form of HA did not show such binding efficiency. The molecular interaction between BMP-2 and HA was determined using molecular dynamic simulations, which demonstrated that at acidic pH molecular interactions were predominantly electrostatic, whereas at the neutral pH, Van der Waals interactions were dominant. Interestingly, these experiments indicated that reconstitution of the BMP-2 in the 3D scaffolds with intrinsic acidic or neutral properties modulate the stability and bioavailability of the growth factor over several weeks. The adsorption and desorption of the protein from HA having different binding mode were quantified by theoretical calculations which correlated well with the experimental release profile of bioactive BMP-2. The theoretical calculations imply that the BMP-2 release from the HA-gel, having neutral pH followed Fick's II law of diffusion, whereas the protein release in acidic gel were controlled by both adsorption and diffusion phenomenon. These calculations also revealed that the neutralization of the acidic gels

leads to complex rearrangement and improve BMP-2 binding to HA by Van der Waals interactions even though the electrostatic interactions were negated. Such interactions were not observed in the neutral gels. In vivo bone induction experiments with these gels clearly demonstrated early mineralization (in just two weeks) in the acidic gel, unlike neutral gels that showed mineralization after six weeks. The total bone volume and bone quality also significantly improved in the acidic gel as compared to that of the neutral gel after eight weeks of experiments. Hence, by subjecting the HA gel and BMP-2 to lower pH promotes molecular interactions that retains and stabilizes the growth factor over several weeks in the gel although it is placed at physiological pH. In summary, this study offers a new insight on 3D matrix fabrication that significantly improves growth factor stability and bioactivity. Such a design increases the bioavailability of the sensitive growth factor that would subsequently reduce the drug dosage and mitigate the associated side effects.

Materials and Methods

Synthesis of hydrazide and aldehyde-modified HA-derivatives

Synthesis of acidic HA-aldehyde and HA-hydrazide derivatives were performed following previously publication (*32*). The HA derivatives were purified by dialysis (Spectra Por-6, MWCO 3500) against dilute HCl (pH=3.5) containing 0.1 M NaCl (2×2L, 48 h), and then dialyzed against deionized water (2×2L, 24 h). The solution was lyophilized to obtain the desired acidic form of HA derivative having the carboxylic acid backbone.

To prepare the neutral form of HA, the dialyzed product mentioned above was neutralized using 0.1 M NaOH and dialyzed against deionized water (2×2L, 24 h).

Hydrogel preparation

HA hydrogel was prepared following previous publication (*32*). Briefly, acidic and neutralized aldehyde and hydrazide derivatives of HA, mentioned above, were dissolved in 10 mM PBS (pH 7.4) at a concentration of 16 mg/mL and sterilized by filtered through 0.45 μm syringe filter (Pall Corp., East Hills, NY). Thereafter, rhBMP-2 was pre-mixed with a HA-hydrazide solution to reach the concentration of 40 μg/mL. The two HA solutions were loaded into two 1 mL syringes with volume ratio of 1:1. The two syringes were connected at the tip with a connector, and the two solutions were mixed ~20 times at room temperature to obtain hydrogel having final BMP-2 concentration of 20 μg/mL. The gel was further kept for 3 h at room temperature before performing in vivo injection.

BMP-2 release from hydrogels

Both acidic and neutral HA hydrogels were prepared as described above. 20 μg BMP-2 was loaded to 200 μL gel. Three gels for each group were prepared individually. Hydrogels were placed into Corning® HTS Transwell®-24 well permeable supports HTS Transwell-24 units w/ 0.4 μm pore polycarbonate membrane and immersed in 800 μL of PBS (total BMP-2 = 20 μg/mL) and incubated at 37 °C. To determine the BMP-2 release from the gels 20 μL of samples were harvested at different time points (day 1, 3, 5, 7, 14, 21, 28). Of the harvested samples, 5 μL of the release medium was added to each well to perform the ALP assay. As a control, 20 μg/mL BMP-2 was suspended in PBS and experiments were repeated in the same way as the BMP-2 release experiment, mentioned above, i.e., 20 μL samples were harvested for each time point to perform the ALP assay (corresponding to 100 ng BMP-2, if 100% released). The

percentage of BMP-2 released at each time point is calculated with respect to the 100% released values obtained from the control experiments.

Cell culture

W-20-17 were maintained in DMEM containing 10% heat inactivated FBS and 1% antibiotics in humidified condition, 37 °C and 5% CO_2. The medium was changed every second day.

ALP activity assay and LDH assay

For ALP activity and LDH activity study W-20-17 were seeded in 96 well plates with a density of 3 000 cells per well. After incubation for 24 h, cell culture medium was replaced by fresh medium containing 5 µL of the harvested samples in 100 µL of DMEM. For each time point, 5 µL of the samples harvested from the control group without hydrogel was also evaluated. The levels of ALP in different cells were evaluated using our previously reported procedure (*9*).

The cell lysate prepared for ALP assay was also used to determine cell number using LDH assay. Briefly, 50 µL LDH substrate (CytoTox 96®Non+radio cytotoxicity, Promega) was added into 20 µL of the remaining lysate and incubated for 20 minutes and the absorbance was measured at 490 nm. The final ALP levels were normalized to the observed LDH level.

Molecular dynamics simulations

Structural models

The atomic coordinates of BMP-2 at pH 7 were obtained from the crystallographic structure (PDB code: 1REW) of a protein complex with its IA receptor (*24*); the protonation state at pH 4.5 was evaluated by means of the H++ software (*25*). Partial atomic charges and force field parameters for BMP-2 were derived from Amberff03 force field (*33*).

The atomic coordinates of HA were obtained through the crystallographic structure (PDB code: 2BVK) (*34*) and replicated in order to build a hexamer, the model chain used to investigate the formation of BMP-2/HA complexes (*35*). All glucuronic acid units are assumed to be ionized; since the pK_a value for HA is equal to 3 (*26*) at pH 4.5 the ratio between dissociated and undissociated glucuronic acid units is about 32. Thus, in this framework, the presence of non-ionized carboxyl moieties can be reasonably neglected.

GLYCAM06 (revision h) (*36*) force field was chosen to model HA oligomers.

Molecular docking

Molecular docking was employed to generate sets of plausible initial geometries for BMP-2/HA complexes at both pH 4.5 and pH 7 since, to the best of our knowledge, there are not crystallographic structures available in literature.

First of all, relaxed structures of both protein and model chain were obtained through a 50 ns molecular dynamics simulation in explicit water at 300 K and 1 bar, using the simulation protocol explained below (*vide infra*). Molecular docking was performed by means of AutoDock Vina software (*37*), which allowed obtaining four input structures. For the sake of completeness, it should be pointed out that BMP-2 protein is a homodimer, with a disulfide bond between two cysteine units that connects the monomers.

All animal experiments were performed in strict accordance to guidelines by FELASA and approved by Uppsala (Sweden) local committee for animal research ethics (C317/10). Male Sprague Dawley rats weighing approximately 400g (n=4) (Scanbur AB, Sollentuna, Sweden) were allowed to acclimatize for one week prior to surgery. Prior to surgery the rats were

weighed and anaesthetized in an induction chamber with 5% isoflurane (Baxter, Sweden), 0.3 L/min oxygen and 0.7 L/min nitrous oxide. The rats were transferred to an anaesthesia mask and the anaesthesia was reduced to 1–2.5% isoflurane, 1 L/min oxygen and 0.8 L/min nitrous oxide and placed on a heated pad during surgery. Each rat was shaved and then washed three times with chlorhexidine (Fresenius Kabi, Uppsala, Sweden). The rat received subcutaneous injection with 4 μg of rhBMP-2 in 200 μL of acidic or neutral HA hydrogels. Each rat received a total of 8 implants, randomly assigned. Animals were subcutaneously administered buprenorfin (Temgesic, Schering-Plough, 0.05 mg/kg) during surgery for postoperative pain mitigation, which was continuously administrated for 3 days.

μ-CT assessment

To quantify the mineralization density of ectopic bone induced by BMP-2 delivered through the acidic and neutral hydrogels, in vivo dynamic scanning at week 1, 2, 4, 6, 8 and ex vivo scanning was performed on the harvested bone samples. SkyScan 1176 (Bruker, Kontich, Belgium) with X-ray source of 90 kV/150 μ and resolution of 36 μm were used for in vivo scanning and 45 kV/552 μA with resolution of 18 μm was used for ex vivo μCT assessment. The projections were reconstructed to cross-sections using NRecon (Bruker, Kontich, Belgium) with correction for misalignment, ring artifacts and beam hardening. The total bone tissue volume of the ectopic bone was determined using CTAn software (Bruker, Kontich, Belgium) applying global threshold. The 3D-reconstructions of samples were achieved by using 3D-DOCTOR 4.0, Able Software.

Histological evaluation

The ex vivo bone samples were fixed by formalin and decalcified by immersing in an electrophoresis system (Tissue-Tek Miles scientific, Histolab, Göteborg, Sweden) containing Osteosoft® decalcifying solution (Merck, Darmstadt, Germany) at room temperature overnight. Bone samples were embedded in paraffin and cut into 5 μm sections. Bone slides were deparaffinized, hydrated and then stained by hematoxylin/eosin (H&E) and Masson's trichrome. The sections were dehydrated and mounted with cover slides, scanned by automated image scanner (Aperio scanscope AT) and analyzed by Aperio ImageScope Software.

Supplementary Materials

Supplementary materials and methods

References and Notes:

1. E. S. Place, N. D. Evans, M. M. Stevens, Complexity in biomaterials for tissue engineering. *Nat. Mater.* **8**, 457-470 (2009).
2. J. S. Silber, D. G. Anderson, S. D. Daffner, B. T. Brislin, J. M. Leland, A. S. Hilibrand, A. R. Vaccaro, T. J. Albert, Donor Site Morbidity After Anterior Iliac Crest Bone Harvest for Single-Level Anterior Cervical Discectomy and Fusion. *Spine* **28**, 134-139 (2003).
3. M. S. Rahman, N. Akhtar, H. M. Jamil, R. S. Banik, S. M. Asaduzzaman, TGF-β/BMP signaling and other molecular events: regulation of osteoblastogenesis and bone formation. *Bone Research* **3**, 15005 (2015).
4. E. J. Carragee, E. L. Hurwitz, B. K. Weiner, A critical review of recombinant human bone morphogenetic protein-2 trials in spinal surgery: emerging safety concerns and lessons learned. *Spine J.* **11**, 471-491.
5. N. E. Epstein, Complications due to the use of BMP/INFUSE in spine surgery: The evidence continues to mount. *Surgical Neurology International* **4**, S343-S352 (2013).

6. H. D. Kim, R. F. Valentini, Retention and activity of BMP-2 in hyaluronic acid-based scaffolds in vitro. *J. Biomed. Mater. Res. Part B* **59**, 573-584 (2002).
7. J. N. Zara, R. K. Siu, X. Zhang, J. Shen, R. Ngo, M. Lee, W. Li, M. Chiang, J. Chung, J. Kwak, B. M. Wu, K. Ting, C. Soo, High Doses of Bone Morphogenetic Protein 2 Induce Structurally Abnormal Bone and Inflammation In Vivo. *Tissue Engineering. Part A* **17**, 1389-1399 (2011).
8. M. Okamoto, J. Murai, H. Yoshikawa, N. Tsumaki, Bone Morphogenetic Proteins in Bone Stimulate Osteoclasts and Osteoblasts During Bone Development. *J. Bone Miner. Res.* **21**, 1022-1033 (2006).
9. M. Kisiel, M. Ventura, O. P. Oommen, A. George, X. F. Walboomers, J. Hilborn, O. P. Varghese, Critical assessment of rhBMP-2 mediated bone induction: An in vitro and in vivo evaluation. *J. Control. Release* **162**, 646-653 (2012).
10. B.-B. Seo, H. Choi, J.-T. Koh, S.-C. Song, Sustained BMP-2 delivery and injectable bone regeneration using thermosensitive polymeric nanoparticle hydrogel bearing dual interactions with BMP-2. *J. Control. Release* **209**, 67-76 (2015).
11. D. E. Discher, D. J. Mooney, P. W. Zandstra, Growth factors, matrices, and forces combine and control stem cells. *Science* **324**, 1673-1677 (2009).
12. E. Martínez-Sanz, D. A. Ossipov, J. Hilborn, S. Larsson, K. B. Jonsson, O. P. Varghese, Bone reservoir: Injectable hyaluronic acid hydrogel for minimal invasive bone augmentation. *J. Control. Release* **152**, 232-240 (2011).
13. O. P. Oommen, S. J. Wang, M. Kisiel, M. Sloff, J. Hilborn, O. P. Varghese, Smart Design of Stable Extracellular Matrix Mimetic Hydrogel: Synthesis, Characterization, and In Vitro and In Vivo Evaluation for Tissue Engineering. *Adv. Funct. Mater.* **23**, 1273-1280 (2013).
14. M. M. Martino, P. S. Briquez, E. Güç, F. Tortelli, W. W. Kilarski, S. Metzger, J. J. Rice, G. A. Kuhn, R. Müller, M. A. Swartz, J. A. Hubbell, Growth Factors Engineered for Super-Affinity to the Extracellular Matrix Enhance Tissue Healing. *Science* **343**, 885-888 (2014).
15. H. Zhang, F. Migneco, C.-Y. Lin, S. J. Hollister, Chemically-Conjugated Bone Morphogenetic Protein-2 on Three-Dimensional Polycaprolactone Scaffolds Stimulates Osteogenic Activity in Bone Marrow Stromal Cells. *Tissue Engineering. Part A* **16**, 3441-3448 (2010).
16. F. Gilde, L. Fourel, R. Guillot, I. Pignot-Paintrand, T. Okada, V. Fitzpatrick, T. Boudou, C. Albiges-Rizo, C. Picart, Stiffness-dependent cellular internalization of matrix-bound BMP-2 and its relation to Smad and non-Smad signaling. *Acta Biomater.* **46**, 55-67 (2016).
17. D. S. Bramono, S. Murali, B. Rai, L. Ling, W. T. Poh, Z. X. Lim, G. S. Stein, V. Nurcombe, A. J. van Wijnen, S. M. Cool, Bone marrow-derived heparan sulfate potentiates the osteogenic activity of bone morphogenetic protein-2 (BMP-2). *Bone* **50**, 954-964 (2012).
18. L. Luca, A.-L. Rougemont, B. H. Walpoth, R. Gurny, O. Jordan, The effects of carrier nature and pH on rhBMP-2-induced ectopic bone formation. *J. Control. Release* **147**, 38-44 (2010).
19. V. Hintze, S. A. Samsonov, M. Anselmi, S. Moeller, J. Becher, M. Schnabelrauch, D. Scharnweber, M. T. Pisabarro, Sulfated Glycosaminoglycans Exploit the Conformational Plasticity of Bone Morphogenetic Protein-2 (BMP-2) and Alter the Interaction Profile with Its Receptor. *Biomacromolecules* **15**, 3083-3092 (2014).
20. O. P. Oommen, C. Duehrkop, B. Nilsson, J. Hilborn, O. P. Varghese, Multifunctional Hyaluronic Acid and Chondroitin Sulfate Nanoparticles: Impact of Glycosaminoglycan Presentation on Receptor Mediated Cellular Uptake and Immune Activation. *ACS Appl. Mater. Interfaces* **8**, 20614-20624 (2016).
21. G. Bhakta, B. Rai, Z. X. H. Lim, J. H. Hui, G. S. Stein, A. J. van Wijnen, V. Nurcombe, G. D. Prestwich, S. M. Cool, Hyaluronic acid-based hydrogels functionalized with heparin that support controlled release of bioactive BMP-2. *Biomaterials* **33**, 6113-6122 (2012).
22. G. Bhakta, Z. X. H. Lim, B. Rai, T. Lin, J. H. Hui, G. D. Prestwich, A. J. van Wijnen, V. Nurcombe, S. M. Cool, The influence of collagen and hyaluronan matrices on the delivery and bioactivity of bone morphogenetic protein-2 and ectopic bone formation. *Acta Biomater.* **9**, 9098-9106 (2013).
23. L. H. Hem, B. Niemeyer, A novel correlation for protein diffusion coefficients based on molecular weight and radius of gyration. *Biotechnol. Prog.* **19**, 544-548 (2003).
24. S. Keller, J. Nickel, J. L. Zhang, W. Sebald, T. D. Mueller, Molecular recognition of BMP-2 and BMP receptor IA. *Nat. Struct. Mol. Biol.* **11**, 481-488 (2004).
25. R. Anandakrishnan, B. Aguilar, A. V. Onufriev, H++3.0: automating pK prediction and the preparation of biomolecular structures for atomistic molecular modeling and simulations. *Nucleic Acids Res.* **40**, W537-W541 (2012).

26. M. B. Brown, S. A. Jones, Hyaluronic acid: a unique topical vehicle for the localized delivery of drugs to the skin. *J. Eur. Acad. Dermatol. Venereol.* **19**, 308-318 (2005).
27. J. Nickel, M. K. Dreyer, T. Kirsch, W. Sebald, The crystal structure of the BMP-2 : BMPR-IA complex and the generation of BMP-2 antagonists. *J. Bone Joint Surg. Am.* **83A**, S7-S14 (2001).
28. W. Sebald, J. Nickel, J. L. Zhang, T. D. Mueller, Molecular recognition in bone morphogenetic protein (BMP)/receptor interaction. *Biol. Chem.* **385**, 697-710 (2004).
29. N. Chennamsetty, V. Voynov, V. Kayser, B. Helk, B. L. Trout, Design of therapeutic proteins with enhanced stability. *Proc. Natl. Acad. Sci. USA* **106**, 11937-11942 (2009).
30. S. Wang, D. Gurav, O. P. Oommen, O. P. Varghese, Insights into the Mechanism and Catalysis of Oxime Coupling Chemistry at Physiological pH. *Chem. Eur. J.* **21**, 5980-5985 (2015).
31. M. R. Todeschi, R. M. E. Backly, O. P. Varghese, J. Hilborn, R. Cancedda, M. Mastrogiacomo, Host cell recruitment patterns by bone morphogenetic protein-2 releasing hyaluronic acid hydrogels in a mouse subcutaneous environment. *Regenerative Medicine* **DOI:10.2217/rme-2017-0023**, null (2017).
32. S. Wang, O. P. Oommen, H. Yan, O. P. Varghese, Mild and efficient strategy for site-selective aldehyde modification of glycosaminoglycans: tailoring hydrogels with tunable release of growth factor. *Biomacromolecules* **14**, 2427-2432 (2013).
33. Y. Duan, C. Wu, S. Chowdhury, M. C. Lee, G. M. Xiong, W. Zhang, R. Yang, P. Cieplak, R. Luo, T. Lee, J. Caldwell, J. M. Wang, P. Kollman, A point-charge force field for molecular mechanics simulations of proteins based on condensed-phase quantum mechanical calculations. *J. Comput. Chem.* **24**, 1999-2012 (2003).
34. A. Almond, P. L. DeAngelis, C. D. Blundell, Hyaluronan: The local solution conformation determined by NMR and computer modeling is close to a contracted left-handed 4-fold helix. *J. Mol. Biol.* **358**, 1256-1269 (2006).
35. A. Pichert, S. A. Samsonov, S. Theisgen, L. Thomas, L. Baumann, J. Schiller, A. G. Beck-Sickinger, D. Huster, M. T. Pisabarro, Characterization of the interaction of interleukin-8 with hyaluronan, chondroitin sulfate, dermatan sulfate and their sulfated derivatives by spectroscopy and molecular modeling. *Glycobiology* **22**, 134-145 (2012).
36. K. N. Kirschner, A. B. Yongye, S. M. Tschampel, J. Gonzalez-Outeirino, C. R. Daniels, B. L. Foley, R. J. Woods, GLYCAM06: A generalizable Biomolecular force field. Carbohydrates. *J. Comput. Chem.* **29**, 622-655 (2008).
37. O. Trott, A. J. Olson, Software News and Update AutoDock Vina: Improving the Speed and Accuracy of Docking with a New Scoring Function, Efficient Optimization, and Multithreading. *J. Comput. Chem.* **31**, 455-461 (2010).
38. J. M. Zuidema, C. J. Rivet, R. J. Gilbert, F. A. Morrison, A protocol for rheological characterization of hydrogels for tissue engineering strategies. *J. Biomed. Mater. Res. Part B* **102**, 1063-1073 (2014).
39. R. B. Bird, W. E. Stewart, E. N. Lightfoot, *Transport phenomena*. (J. Wiley, New York, ed. 2nd, Wiley international, 2002), pp. xii, 895 p.
40. S. Pronk, S. Pall, R. Schulz, P. Larsson, P. Bjelkmar, R. Apostolov, M. R. Shirts, J. C. Smith, P. M. Kasson, D. van der Spoel, B. Hess, E. Lindahl, GROMACS 4.5: a high-throughput and highly parallel open source molecular simulation toolkit. *Bioinformatics* **29**, 845-854 (2013).
41. W. L. Jorgensen, J. Chandrasekhar, J. D. Madura, R. W. Impey, M. L. Klein, Comparison of simple potential functions for simulating liquid water *J. Chem. Phys.* **79**, 926 - 936 (1983).
42. I. S. Joung, T. E. Cheatham, Molecular Dynamics Simulations of the Dynamic and Energetic Properties of Alkali and Halide Ions Using Water-Model-Specific Ion Parameters. *J. Phys. Chem. B* **113**, 13279-13290 (2009).
43. I. S. Joung, T. E. Cheatham, Determination of alkali and halide monovalent ion parameters for use in explicitly solvated biomolecular simulations. *J. Phys. Chem. B* **112**, 9020-9041 (2008).
44. C. Zhang, S. Raugei, B. Eisenberg, P. Carloni, Molecular Dynamics in Physiological Solutions: Force Fields, Alkali Metal Ions, and Ionic Strength. *Journal of Chemical Theory and Computation* **6**, 2167-2175 (2010).
45. U. Essmann, L. Perera, M. L. Berkowitz, T. Darden, H. Lee, L. G. Pedersen, A Smooth Particle Mesh Ewald Method. *J. Chem. Phys.* **103**, 8577-8593 (1995).
46. T. Darden, D. York, L. Pedersen, Particle Mesh Ewald - an N.Log(N) Method for Ewald Sums in Large Systems. *J. Chem. Phys.* **98**, 10089-10092 (1993).
47. B. Hess, H. Bekker, H. J. C. Berendsen, J. G. E. M. Fraaije, LINCS: A linear constraint solver for molecular simulations. *J. Comput. Chem.* **18**, 1463-1472 (1997).

48. G. Bussi, D. Donadio, M. Parrinello, Canonical sampling through velocity rescaling. *J. Chem. Phys.* **126**, (2007).
49. M. Parrinello, A. Rahman, Polymorphic Transitions in Single-Crystals - a New Molecular-Dynamics Method. *J. Appl. Phys.* **52**, 7182-7190 (1981).
50. D. A. Case, T. A. Darden, T. E. Cheatham, III, C. L. Simmerling, J. Wang, R. E. Duke, R. Luo, M. Crowley, R. C. Walker, W. Zhang, K. M. Merz, B. Wang, S. Hayik, A. Roitberg, G. Seabra, I. Kolossvàry, K. F. Wong, F. Paesani, J. Vanicek, X. Wu, S. R. Brozell, T. Steinbrecher, H. Gohlke, L. Yang, C. Tan, J. Mongan, V. Hornak, G. Cui, D. H. Mathews, M. G. Seetin, C. Sagui, V. Babin, P. A. Kollman. (University of California, San Francisco, 2008).
51. B. R. Miller, T. D. McGee, J. M. Swails, N. Homeyer, H. Gohlke, A. E. Roitberg, MMPBSA.py: An Efficient Program for End-State Free Energy Calculations. *Journal of Chemical Theory and Computation* **8**, 3314-3321 (2012).
52. N. A. Baker, D. Sept, S. Joseph, M. J. Holst, J. A. McCammon, Electrostatics of nanosystems: Application to microtubules and the ribosome. *P. Natl. Acad. Sci. USA* **98**, 10037-10041 (2001).

Acknowledgement
The present work was supported by Swedish Strategic Research grant "StemTherapy" (139400126), Swedish foundation for strategic research (SSF) grant (139400127) and EU Framework Program-7 project "Biodesign (NMP3-LA-2011-262948)." The authors acknowledge China Scholarship Council (CSC) for supporting HY. We sincerely thank Ms. Brittmarie Andersson for performing in vivo studies and CT scanning. We also acknowledge the computational resources from ETH Zurich with Brutus and Euler clusters.

Author contributions

OPV conceived the project, designed experiments, analysed the results and wrote the manuscript together with TC; HY participated in in vivo experiments, performed BMP-2 release and histochemical analysis and contributed in writing the experimental part; TC and MS performed computational analysis and edited the computational part; GHB participated in in vivo experiments and edited the manuscript; SW prepared HA hydrogels, performed swelling and rheological studies and edited the hydrogel part; OPO, SL and JH participated in scientific discussion and edited the manuscript

Figures

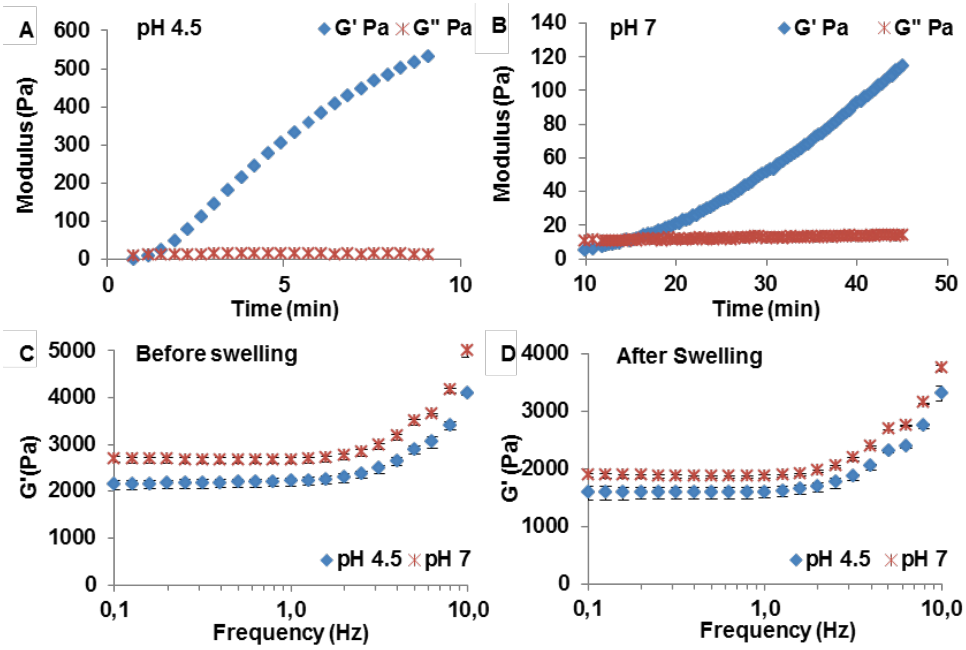

Fig. 1. Rheological evaluation of the acidic and neutral HA hydrogels. Insert (A, B) represents gelling kinetics whereas insert (C, D) represents mechanical properties of acidic and neutral hydrogels before and after swelling in phosphate buffer.

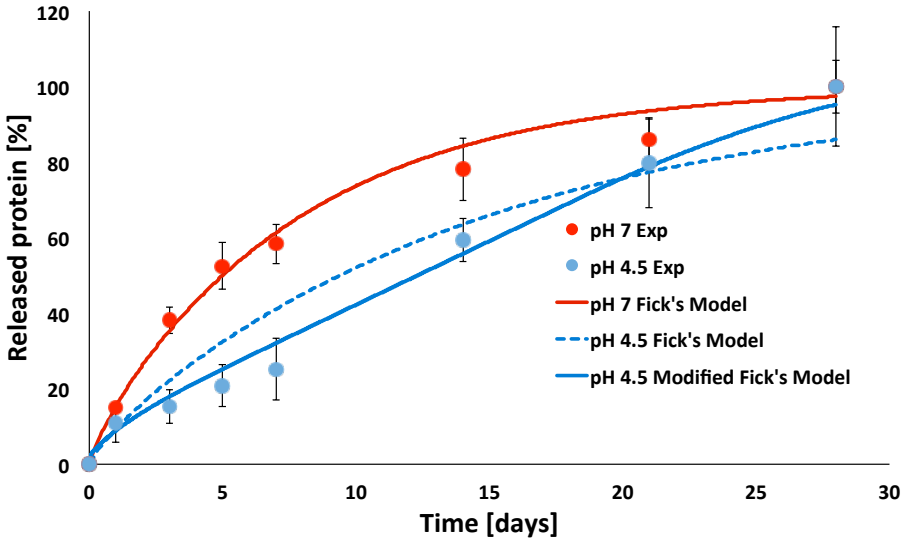

Fig. 2. Experimental release of bioactive BMP-2 is indicated by marked scatter plot from acidic (blue) and neutral (red) gels. Continuous line corresponds to the theoretical release according to the Fick's II law of diffusion, whereas the dotted lines represent the modified Fick's model. In vitro release of bioactive BMP-2 was determined from the ALP activity assay in response to released rhBMP-2 from the acidic and neutral HA hydrogels for up to 28 days in W-20-17 cells. Data are shown as an average of triplicate wells from three individual experiments.

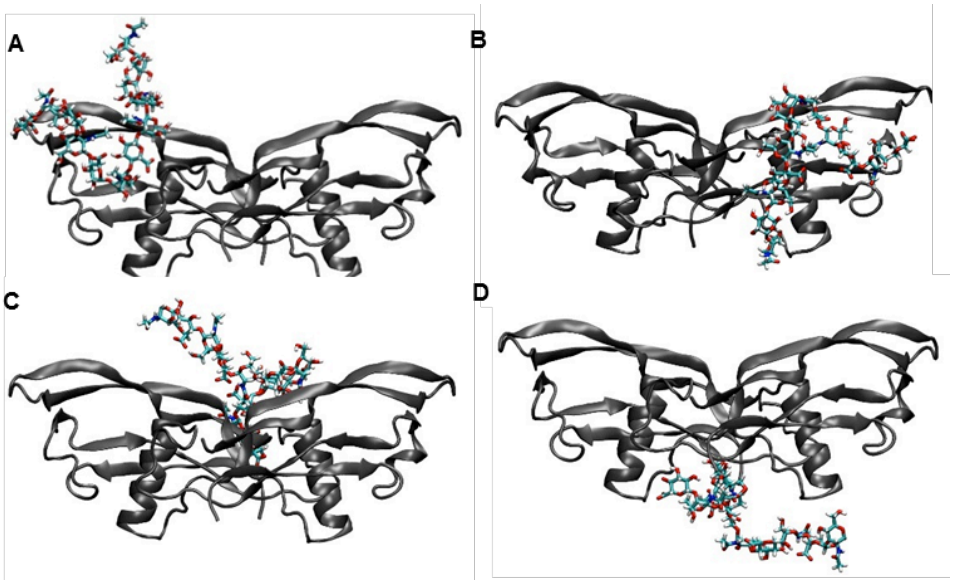

Fig. 3. Examples of input HA–BMP-2 complex structures: (A) wrist, (B) knuckle, (C) upper and (D) lower geometries.

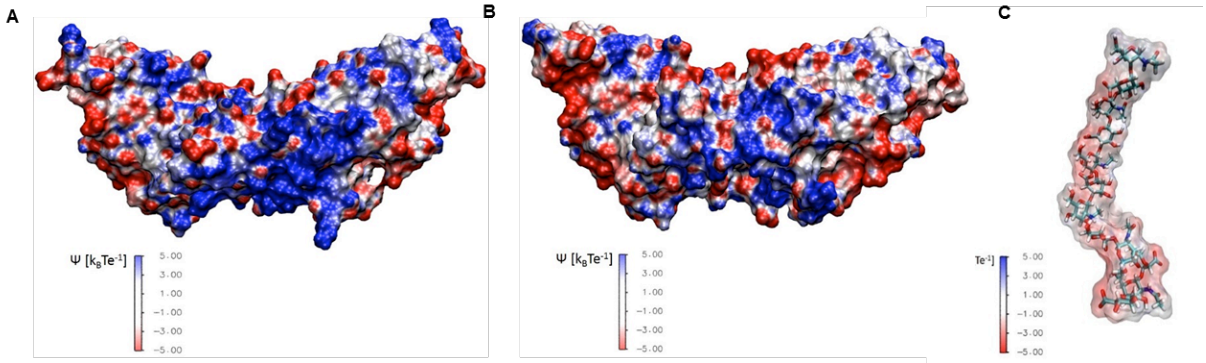

Fig. 4. Electrostatic potential maps of BMP-2 at (A) pH 4.5, (B) at pH 7 and that of (C) HA at pH 7. Electrostatic potential ψ is expressed in $kBTe^{-1}$ unit.

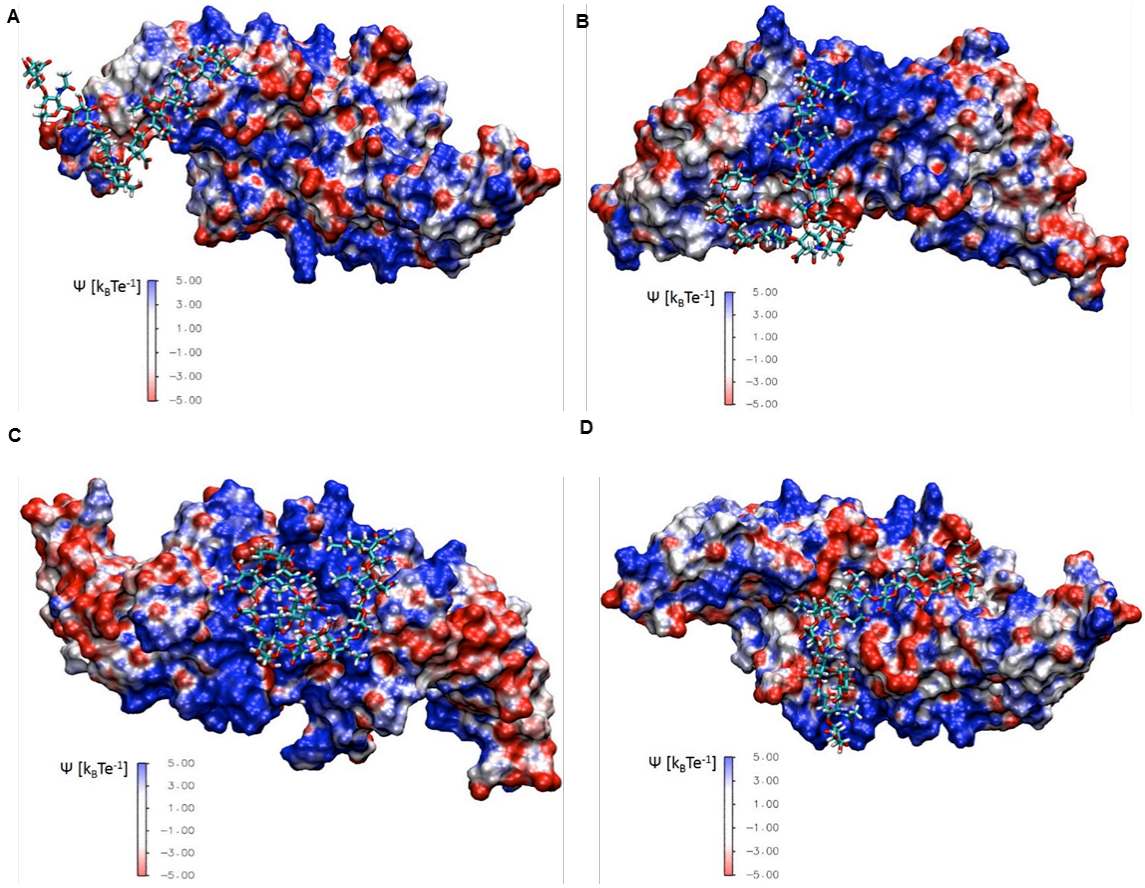

Fig. 5. Representative HA–BMP-2 complex structures along with electrostatic potential maps relative to BMP-2 at pH 4.5: (A) wrist, (B) knuckle (C) lower and (D) upper. Electrostatic potential ψ is expressed in k_BTe^{-1} unit.

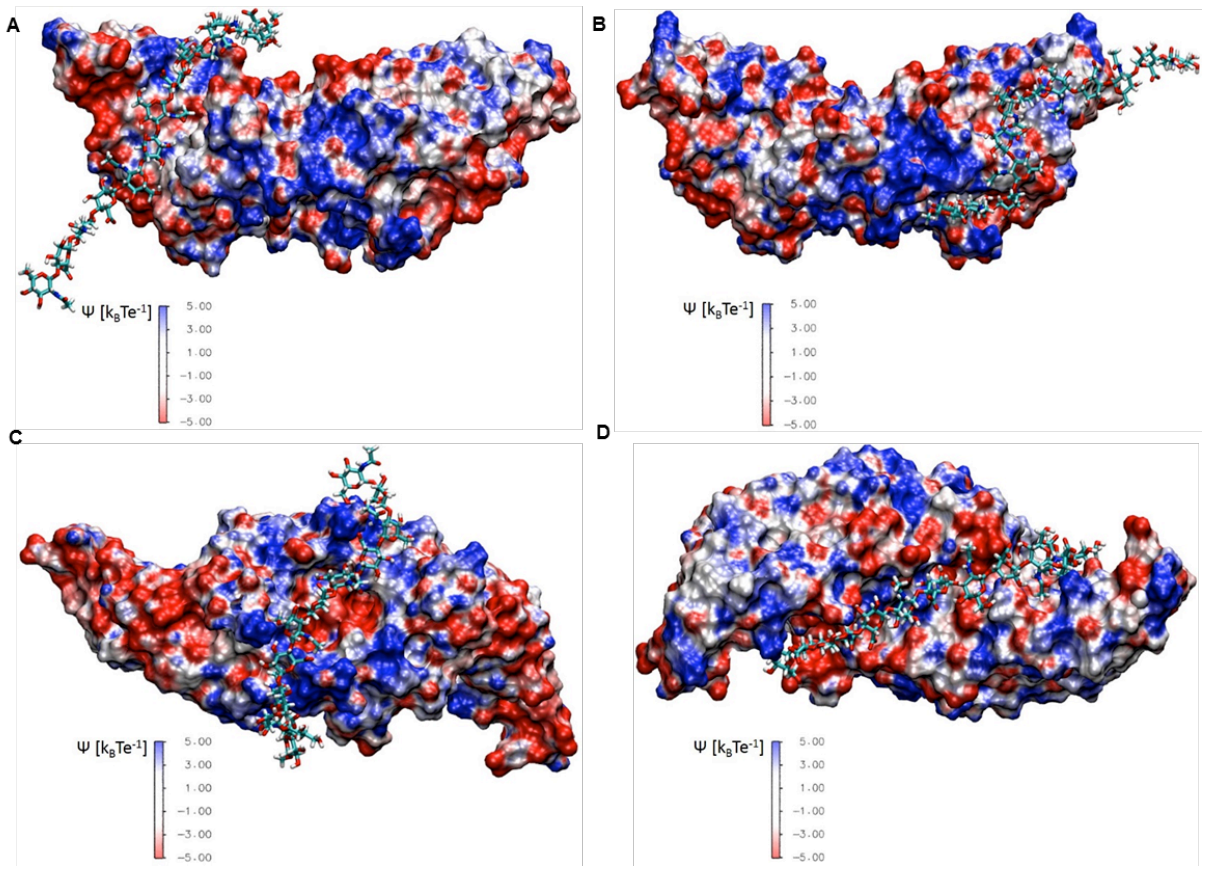

Fig. 6. Representative HA–BMP-2 complex structures along with electrostatic potential maps relative to BMP-2 at pH 7: (A) wrist, (B) knuckle (C) lower and (D) upper. Electrostatic potential ψ is expressed in k_BTe^{-1} unit.

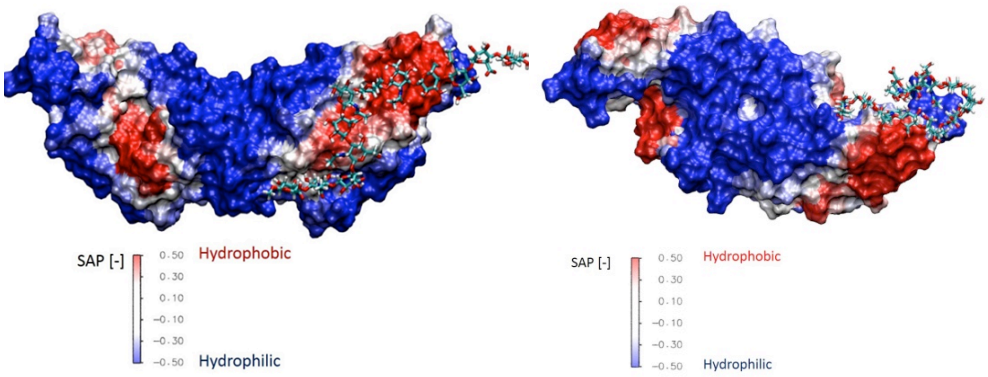

Fig. 7. Hydrophobic interactions in HA–BMP-2 complexes in the (A) knuckle and (B) wrist structures along with hydrophobic patches relative to BMP-2 (after neutralization) at pH 7.

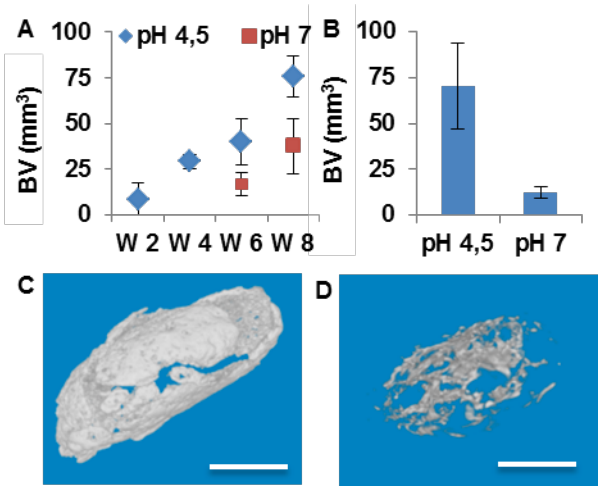

Fig. 8. Ectopic bone volume (BV) was quantitatively evaluated by micro CT (μCT) after implantation of acidic and neutral hydrogels in a rat model. (A) The dynamic μCT analysis in live animal at different time points indicating differences in BV observed in the acidic and neutral hydrogels (week 2 to week 8). (B) Ex vivo quantitative μCT analysis of ectopic bone tissues harvested at week 8. (C, D) Representatives of 3D reconstruction of images obtained from μCT after 8 weeks in acidic and neutral hydrogels respectively. Scale bar = 500 μm.

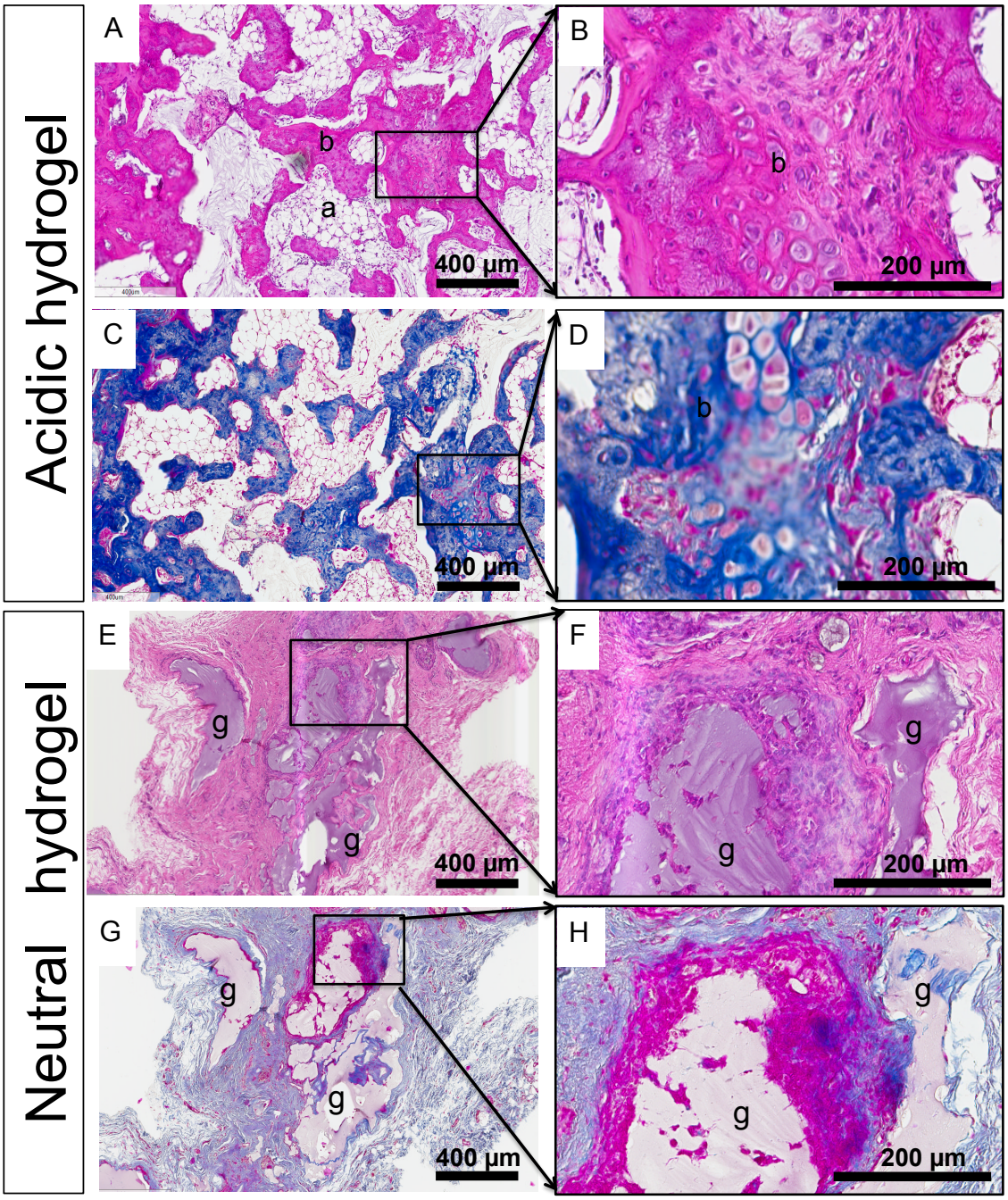

Fig. 9. Histological evaluation of *de novo* bone induced by subcutaneous injection of rhBMP-2 loaded acidic hydrogels (A, B, C, D) and neutral hydrogels (E, F, G, H) that were harvested after eight weeks of implantation. Hematoxylin/eosin (H&E) (A, B, E, F) and Masson's trichrome (C, D, G, H) staining were evaluated on paraffin-embedded cross sections. The abbreviations ‘a’ indicate adipocytes; ‘b’ indicates matured bone; and ‘g’ indicates remnant hydrogels.

Table 1. Physical properties of acidic and neutral HA hydrogels before and after swelling

	Before swelling				After swelling		sw%	HAse* (h)
	G' (Pa)	G'' (Pa)	ξ (nm)	Mc (kg/mol)	G' (Pa)	G'' (Pa)		
pH 4.5	2150±94	13.4±0.5	12.4	18.0	1574±105	14.0±1.1	24.8±3.4	20
pH 7	2657±60	14.6±1.7	11.6	14.6	1867±28	12.1±0.6	28.1±3.0	25

Table 2. Fitting parameters for diffusion and diffusion/desorption models

	pH 7	pH 4.5 (diffusion model)	pH 4.5 (diffusion/desorption model)
D [$cm^2\ s^{-1}$]	$4.11 \cdot 10^{-7}$	$2.19 \cdot 10^{-7}$	$1.2 \cdot 10^{-6}$
k_{des} [s^{-1}]	-	-	$3.47 \cdot 10^{-6}$
C_b [μmol cm^{-3}]	0	0	0
$C_{protein,eq}$ [μmol cm^{-3}]	-	-	$7.14 \cdot 10^{-4}$

Table 3. Interaction energies for each HA–BMP-2 complex at pH 4.5 and pH 7, along with specific electrostatic and Van der Waals contributions. Values are expressed as average ± standard error

	ΔE (kcal mol^{-1})	Wrist	Knuckle	Lower	Upper
pH 4.5	Electrostatic	-399.85 ± 4.65	-588.48 ± 1.90	-1009.29 ± 3.85	-703.30 ± 1.80
	Van der Waals	-33.07 ± 0.51	-53.46 ± 0.23	-42.24 ± 0.41	-79.94 ± 0.29
	Total	-16.25 ± 0.49	-33.50 ± 0.40	-33.68 ± 0.46	-39.66 ± 0.47
pH 7	Electrostatic	664.55 ± 3.12	361.26 ± 4.12	-86.95 ± 3.60	708.41 ± 3.56
	Van der Waals	-48.82 ± 0.69	-65.26 ± 0.61	-74.88 ± 0.68	-98.07 ± 0.71
	Total	-12.43 ± 0.79	-26.67 ± 0.60	-47.91 ± 0.89	-9.61 ± 0.93

Table 4. Interaction energies for each complex after neutralization, along with specific electrostatic and Van der Waals contributions. Values are expressed as the average ± standard error

ΔE (kcal mol^{-1})	Wrist	Knuckle	Lower	Upper
Electrostatic	453.59 ± 3.07	383.27 ± 1.60	-222.54 ± 5.08	425.02 ± 2.75
Van der Waals	-42.20 ± 0.55	-59.39 ± 0.31	-79.52 ± 0.51	-75.38 ± 0.24
Total	-11.12 ± 1.18	-1.39 ± 0.73	-46.95 ± 0.96	-25.36 ± 0.64